

# BRAIN COMMUNICATIONS

## Amyloid precursor protein processing in human neurons with an allelic series of the *PSEN1* intron 4 deletion mutation and total presenilin-1 knockout

Charles Arber,<sup>1</sup> Claudio Villegas-Llerena,<sup>1,2</sup> Jamie Toombs,<sup>1,3</sup> Jennifer M. Pocock,<sup>2</sup> Natalie S. Ryan,<sup>4</sup> Nick C. Fox,<sup>1,3,4</sup> Henrik Zetterberg,<sup>1,3,5,6</sup> John Hardy<sup>1,3</sup> and Selina Wray<sup>1</sup>

Mutations in presenilin-1 (*PSEN1*), encoding the catalytic subunit of the amyloid precursor protein-processing enzyme  $\gamma$ -secretase, cause familial Alzheimer's disease. However, the mechanism of disease is yet to be fully understood and it remains contentious whether mutations exert their effects predominantly through gain or loss of function. To address this question, we generated an isogenic allelic series for the *PSEN1* mutation intron 4 deletion; represented by control, heterozygous and homozygous mutant induced pluripotent stem cells in addition to a presenilin-1 knockout line. Induced pluripotent stem cell-derived cortical neurons reveal reduced, yet detectable amyloid-beta levels in the presenilin-1 knockout line, and a mutant gene dosage-dependent defect in amyloid precursor protein processing in *PSEN1* intron 4 deletion lines, consistent with reduced processivity of  $\gamma$ -secretase. The different effects of presenilin-1 knockout and the *PSEN1* intron 4 deletion mutation on amyloid precursor protein-C99 fragment accumulation, nicastrin maturation and amyloid-beta peptide generation support distinct consequences of familial Alzheimer's disease-associated mutations and knockout of presenilin-1 on the function of  $\gamma$ -secretase.

1 Department of Neurodegenerative Disease, UCL Queen Square Institute of Neurology, London WC1N 1PJ, UK

2 Department of Neuroinflammation, UCL Queen Square Institute of Neurology, London WC1N 1PJ, UK

3 UK Dementia Research Institute at UCL, London, UK

4 Department of Neurodegenerative Disease, Dementia Research Centre, UCL Queen Square Institute of Neurology, London WC1N 1PJ, UK

5 Department of Psychiatry and Neurochemistry, Institute of Neuroscience and Physiology, The Sahlgrenska Academy, University of Gothenburg, Mölndal, Sweden

6 Clinical Neurochemistry Laboratory, Sahlgrenska University Hospital, Mölndal, Sweden

Correspondence to: Selina Wray, PhD, Department of Neurodegenerative Disease

UCL Queen Square Institute of Neurology

1 Wakefield Street, London WC1N 1PJ, UK

E-mail: selina.wray@ucl.ac.uk

**Keywords:** Alzheimer's disease; iPSCs; CRISPR/Cas9; amyloid beta

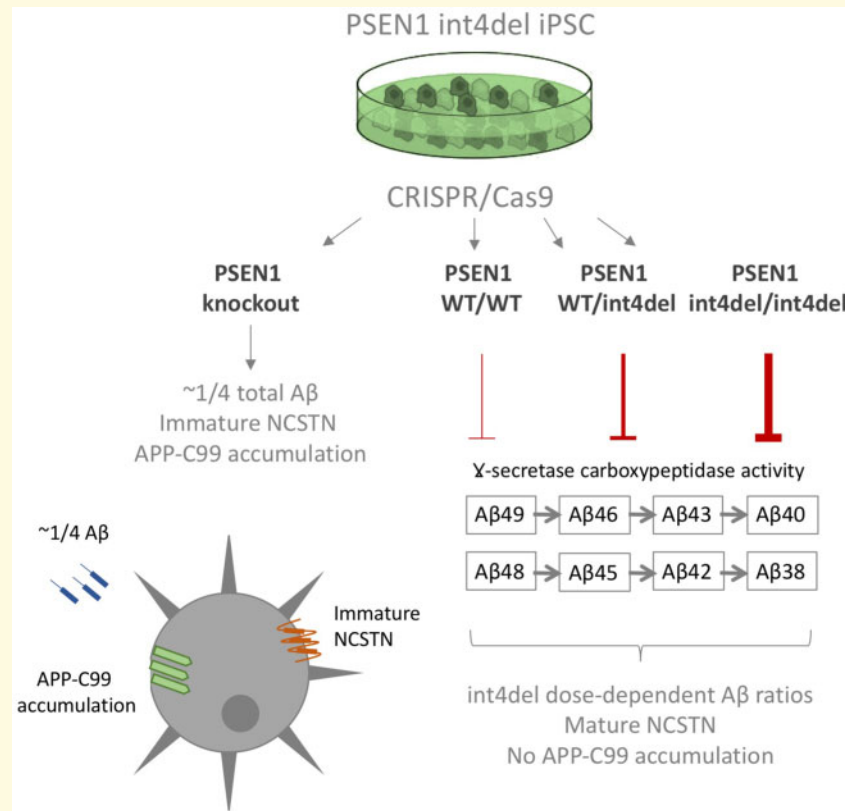
**Abbreviations:**  $\beta$  = amyloid beta; PP = amyloid precursor protein; CRISPR = clustered regularly interspersed short palindromic repeats; DAPT =  $\gamma$ -secretase inhibitor N-[N-(3, 5-Difluorophenyl)-L-alanyl]-S-phenylglycine t-butyl ester; fAD = familial Alzheimer's disease; iPSC = induced pluripotent stem cell; NCSTN = nicastrin; PSEN1/2 = presenilin-1 or presenilin-2; RFLP = restriction fragment length polymorphism; sgRNA = single guide RNA; ssODN = single-stranded oligodeoxynucleotide

Received July 04, 2019. Revised September 06, 2019. Accepted September 11, 2019. Advance Access publication October 14, 2019

© The Author(s) (2019). Published by Oxford University Press on behalf of the Guarantors of Brain.

This is an Open Access article distributed under the terms of the Creative Commons Attribution License (<http://creativecommons.org/licenses/by/4.0/>), which permits unrestricted reuse, distribution, and reproduction in any medium, provided the original work is properly cited.

## Graphical Abstract



## Introduction

Amyloid precursor protein (APP) is cleaved by  $\gamma$ -secretase, the catalytic subunit of which consists of presenilin-1 (PSEN1) or presenilin-2 (PSEN2), to produce amyloid  $\beta$  (A $\beta$ ). Mutations in *APP* and *PSEN1/2* that cause familial Alzheimer's disease (fAD) are believed to alter this interaction, increasing the relative proportion of aggregation-prone A $\beta$  species (Ryan *et al.*, 2016), and forming the basis of the amyloid cascade hypothesis (Hardy and Allsop, 1991).

PSEN1 and PSEN2 are alternate catalytic subunits of  $\gamma$ -secretase, a tetrameric protein complex also containing nicastrin (NCSTN), PSEN enhancer (PEN2) and alternate subunits anterior pharynx 1a/b (APH1a/b; De Strooper, 2003).  $\gamma$ -Secretase serves as a membrane protease, cleaving numerous substrates (Haapasalo and Kovacs, 2011) that include the products of  $\beta$ -secretase and  $\alpha$ -secretase cleavage of APP (C99 and C83, respectively). Cleavage of C99 by  $\gamma$ -secretase occurs through an initial endopeptidase-like activity followed by subsequent carboxypeptidase-like cleavages to generate shorter A $\beta$  fragments (Takami *et al.*, 2009; Matsumura *et al.*, 2014). In addition,  $\gamma$ -secretase-independent activities for PSEN1 have been described, such as a chaperone activity crucial for the glycosylation and maturation of NCSTN (Leem *et al.*, 2002).

*PSEN1* mutations have been shown to consistently reduce the carboxypeptidase-like activity of  $\gamma$ -secretase, leading to the accumulation of longer, more amyloidogenic A $\beta$  species, such as A $\beta$ 42 and A $\beta$ 43 (Chávez-Gutiérrez *et al.*, 2012; Szaruga *et al.*, 2015; Arber *et al.*, 2019). This can be evidenced as an increased A $\beta$ 42:38 ratio (Takami *et al.*, 2009; Matsumura *et al.*, 2014). The *PSEN1* intron 4 deletion mutation (L113\_I114insT; hereafter referred to as int4del) describes the deletion of a guanine nucleotide in the splice donor region of *PSEN1* after exon 4 leading to three alternative transcripts; one coding a full-length protein with an insertion of an additional threonine in the PSEN1 protein, and two shorter transcripts with premature stop codons (De Jonghe *et al.*, 1999). The long transcript was shown to be responsible for elevated A $\beta$ 42 generation (De Jonghe *et al.*, 1999). We and others have previously shown that this mutation increases the A $\beta$ 42:38 ratio in patient-derived iPSC-neurons and potentially reduces overall  $\gamma$ -secretase activity (Moore *et al.*, 2015; Arber *et al.*, 2019).

There has been contention over the question of whether mutant *PSEN1* alleles confer predominantly gain or loss of function (Veugelen *et al.*, 2016; Xia *et al.*, 2016). In order to further investigate the molecular mechanisms of the *PSEN1* int4del mutation in a human neuronal system, we used CRISPR/Cas9 gene editing to produce an isogenic allelic series from patient-derived iPSCs. The

series is represented by isogenic control (wild type) cells, heterozygous and homozygous mutation-bearing cells, as well as PSEN1 knockout cells. We find that iPSC-derived cortical neurons maintain A $\beta$  generation in PSEN1 knockout cells and display a mutant gene dosage-dependent phenotype on APP/A $\beta$  processing and A $\beta$ 42 generation. The data support distinct effects of fAD-associated mutations and PSEN1 protein knockout.

## Materials and methods

### Cell culture

The acquisition of patient fibroblasts for the generation of iPSC was approved by the National Hospital for Neurology and Neurosurgery and Institute of Neurology Joint Research Ethics Committee (Study Title: Induced pluripotent stem cells derived from patients with familial Alzheimer's disease and other dementias as novel cell models for neurodegeneration, Reference: 09/H0716/64).

All reagents are from ThermoFisher unless specified. PSEN1 int4del iPSCs were obtained from StemBanc and cultured in Essential 8 media on Geltrex substrate and passaged using 0.5 mM EDTA, with the exception of gene editing steps that were performed in mTESR media (Stem Cell Technologies). Differentiation was performed following published protocols (Shi *et al.*, 2012). In brief, iPSCs were grown to confluency and switched to N2B27 media containing 10  $\mu$ M SB431542 and 1  $\mu$ M dorsomorphin (both Tocris). N2B27 media is composed of a mix of 1:1 DMEM-F12 and Neurobasal supplemented with 0.5 $\times$  N2 supplement, 0.5 $\times$  B27 supplement, 0.5 $\times$  non-essential amino acids, 1 mM L-glutamine, 25 U pen/strep, 10  $\mu$ M  $\beta$ -mercaptoethanol and 25 U insulin. Following 10 days of neural induction, cells were maintained in N2B27 without SB431542 and dorsomorphin until day 100, which was taken as the final time point for neuronal analysis. DAPT (Tocris) treatment was performed with 10  $\mu$ M DAPT for 48 h.

### Karyotype analysis

Genomic DNA from iPSC lines was tested using the hPSC Genetic Analysis Test (Stem Cell Technologies). Analysis of the eight most common PSC mutation sites showed there were no significant chromosomal abnormalities in the four iPSC lines. Results highlight possible, non-significant abnormalities that are believed to be PCR artefacts.

### CRISPR/Cas9-mediated genome editing

sgRNAs were designed and constructed using the CRISPR finder tool from the WTSI Genome Editing (WGE) website (Hodgkins *et al.*, 2015). The single-

stranded donor oligonucleotide (ssODN, Table 1), used as homologous recombinant template, was designed to correct the int4del mutation in the heterozygous patient cells. ssODN was asymmetric (60 and 35 bp to the 5' and 3' ends of the double-strand break, respectively) and was synthesized with phosphorothioate modifications (IDT) to increase the efficiency of homology-directed DNA repair (Renaud *et al.*, 2016). For CRISPR/Cas9 gene editing, we used the RNP (ribonucleoprotein) delivery strategy. RNP preparation was performed as per the manufacturer's protocol using the Alt-R<sup>TM</sup> CRISPR tracrRNA, crRNA and S.p. Cas9 Nuclease 3NLS (IDT). Both the ssODN and the RNP were delivered simultaneously into patient-derived iPSCs by electroporation (Amaxa 4D, Lonza). Transfected cells were seeded and expanded in mTESR media + 10  $\mu$ M ROCK inhibitor (Stem Cell Technologies). Screening of modified clones was performed by restriction fragment length polymorphism (RFLP) using the RsaI enzyme, which specifically cleaves the WT and not the int4del pathogenic allele. Edited clones were confirmed by polymerase chain reaction (PCR) and Sanger sequencing. Off-target sites were predicted using the CRISPR finder tool and the sgRNA sequence used for gene editing. PCR primers were designed for the amplification of the top-5 potential off-target sites (Table 1). Sanger sequencing screening of our isogenic allelic series of iPSC cells showed no evidence of off-target activity at any of the screened loci. Sequence alignment was performed using SnapGene software and chromatograms with frame shift mutations were deconvoluted using the Indigo programme (gear.embl.de/indigo/).

### Immunocytochemistry

Cells were fixed for 15 min in 4% paraformaldehyde. Following fixation, cells were washed three times in PBS with 0.3% Triton-X-100 (PBST) and blocked in 3% bovine serum albumin in PBST for 20 min. Primary antibodies (Table 2) were added to cells overnight at 4°C in blocking solution. Cells were washed three times in PBST and Alexafluor secondary antibodies were added in blocking solution for 1 h at room temperature. Following three final washes in PBST (the first of which contained DAPI nuclear counterstain), cells were mounted in fluorescence mounting media (DAKO) and imaged on a Zeiss LSM microscope.

### Polymerase chain reaction

RNA was isolated from neurons using Trizol reagent following the manufacturer's protocols. cDNA was generated using superscript IV following the manufacturers' protocols with 2  $\mu$ g of total RNA and using random hexamer primers. PCR was performed using GoTaq PCR mastermix (Promega). Quantitative PCR (qPCR) was performed using Power SYBR green and an MX3000P thermocycler (Agilent). Primers are shown in Table 1.

**Table 1 Primers used in this study**

|                        | Assay           | Forward  | Reverse                  |
|------------------------|-----------------|--|--------------------------|
| PSEN1 int4del specific | PCR (gDNA)      | CGGAAGGATGGGCAGCTTACA  | AGCCACGCAGTCCATTGAGG     |
| PSEN1 exon 4 splicing  | PCR (cDNA)      | TGAGGACAACACCTGAGCAA   | TGGCAGCATTGAGAATTGAGT    |
| PSEN1                  | Sequencing/RFLP | AGGTCTAACCGTTACCTTGATTC  | CAGCCCTATCCAGTAATACCATAC |
| ssODN                  | CRISPR/Cas9     | T*C*TCTGCATGGTGGTGGTGGTGGCTACCATTAAAGTCAGTCAGCTTTTATACCC<br>GGAAGGATGGGCAGCTGTACGTATGAGTTTTGTTTTATTA*T*T |                          |
| sgRNA                  | CRISPR/Cas9     | AGCTTTTATACCCGGAAGGA   |                          |
| Off-target 1           | Sequencing      | CACAGCGTTACGTTGTATTG   | CCAGGGAAGAAACAGAGACTAAC  |
| Off-target 2           | Sequencing      | ACAAGTAGACTTCTAGGCTGAAAC   | CATGACTTCCTGAGGAGAACAG   |
| Off-target 3           | Sequencing      | TAGGTAAACACTGGCTGGAAAG   | AGCAAGTGGGAAAGAAGACC     |
| Off-target 4           | Sequencing      | GCCTGCGATTTGAGGGATAAC  | AGTTAAAGGGAGCAGGGACTAC   |
| Off-target 5           | Sequencing      | GAATCCTCCAGCCGGTCTTC   | CAGCCCTGTCCCACCTTTC      |
| RPL18a                 | qPCR            | CCCACAACATGTACCGGGAA   | TCTTGGAGTCGTGGAAGTGC     |
| APP                    | qPCR            | GGTACCCACTGATGGTAAT  | GGTAGACTTCTTGGCAATAC     |
| PSEN1                  | qPCR            | TATCAAGTACCTCCCTGAAT   | ACCATTGTTGAGGAGTAAAT     |
| PSEN2                  | qPCR            | ATCTCTGTGTATGATCTCGT   | TCCCCAAAAGTGTCTATAG      |
| BACE1                  | qPCR            | GTCTCTGGTATACACCCATC   | CATAGTTGTACTCCTTGCAG     |
| TUBB3                  | qPCR            | CATGGACAGTGTCCGCTCAG   | CAGGCAGTCGCAGTTTTCAC     |
| TBR1                   | qPCR            | AGCAGCAAGATCAAAAGTGAGC   | ATCCACAGACCCCTCACTAG     |
| CTIP2                  | qPCR            | CTCCGAGCTCAGGAAAGTGTC  | TCATCTTTACCTGCAATGTTCTCC |
| ECE1                   | qPCR            | AGTGACACAGAAAACAACCT   | GAACTGCAGTGTAGTCATTAAA   |
| ACE                    | qPCR            | GAAGTTTGATGTGAACCACT   | ACAGGATCTTGTGTACTCCT     |
| IDE                    | qPCR            | CAAAGACTCACTCAACGAG  | CTGAAAGATACATCCCATAG     |
| NEP                    | qPCR            | GAGGGGTACGATTTTAG  | AAGTCTGTACAAGGCTCAGT     |

\*Phosphorothioate modification.

**Table 2 Antibodies used in this study**

| Antibody     | Company                          | Species          |
|--------------|----------------------------------|------------------|
| SSEA4        | Biologend MC-813–70              | Mouse            |
| OCT4         | SantaCruz sc5297                 | Goat             |
| TUJ1         | Biologend 801201 and 802001      | Mouse and rabbit |
| TBR1         | Abcam ab31940                    | Rabbit           |
| APP 6e10     | Biologend 803014                 | Mouse            |
| APP C-term   | Biologend 802803                 | Mouse            |
| PSEN1 N-term | Millipore MAB1563                | Rat              |
| PSEN1 C-term | Millipore MAB5232                | Mouse            |
| PSEN2        | Cell Signaling Technologies 9979 | Rabbit           |
| NCSTN        | BD Transduction Labs 612290      | Mouse            |
| Actin        | Sigma 1978                       | Mouse            |

## Western blotting

Cells were lysed in RIPA buffer containing protease and phosphatase inhibitors (Roche). Lysates were denatured in NuPage LDS buffer and loaded onto 4–12% precast polyacrylamide gels in MES running buffer (NuPage/ThermoFisher). Proteins were transferred to a nitrocellulose membrane, blocked in 3% bovine serum albumin and blotted using antibodies in Table 2. Images were taken and analysed on an Odyssey Fc (LiCor Biosciences).

## A $\beta$ -Electrochemiluminescence

Forty-eight hours conditioned media were collected from neuronal cultures and centrifuged to remove cell debris. A $\beta$ 42, A $\beta$ 40 and A $\beta$ 38 were quantified simultaneously using the Meso Scale Discovery V-Plex A $\beta$  peptide panel

kit (6E10) by electrochemiluminescence. Samples were diluted 1:1 with diluent 35 and measurements were made on the MSD Sector 6000. A $\beta$  concentrations in the cell media were normalized to cell pellet protein concentration, measured using BioRad BCA assay.

## Statistical analysis

Data analysis was performed in Microsoft Excel and GraphPad Prism 7. Samples were compared via one-way ANOVA with subsequent *post hoc* Tukey's multiple comparisons test (\* $P > 0.05$ , \*\* $P > 0.01$ , \*\*\* $P > 0.001$ , \*\*\*\* $P > 0.0001$ ). Error bars on histograms show  $\pm$  standard deviation of the mean and independent experimental replicates are shown via numbers within histograms.

## Data availability

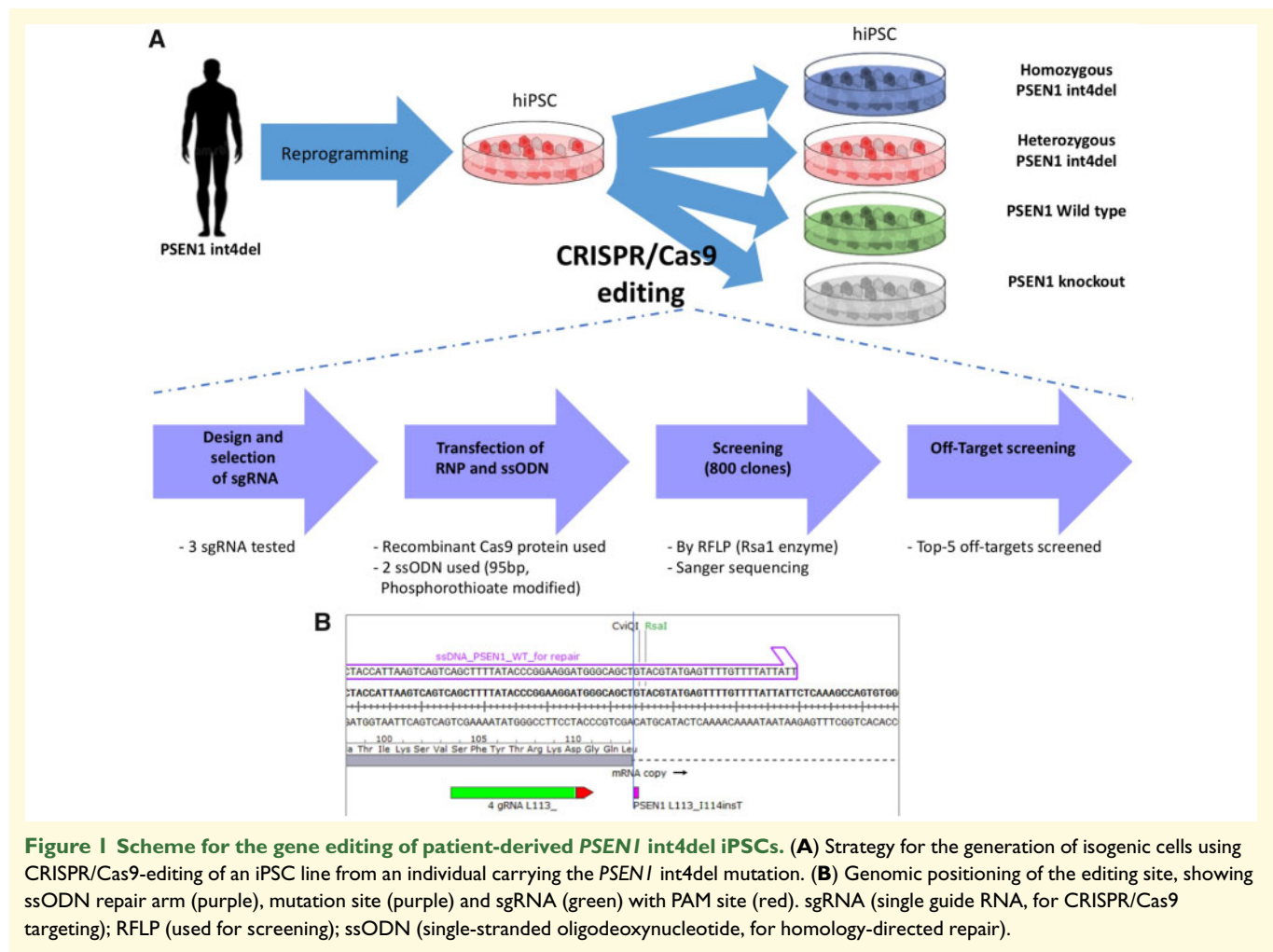
The authors confirm that all the data supporting the findings of this study are available within the article and readily available upon request. For ANOVA analyses, exact  $P$ -values,  $F$ -values and degrees of freedom are presented in the [Supplementary material](#).

## Results

### Generation of PSEN1 int4del allelic series

CRISPR/Cas9 gene editing was used to generate an isogenic series of iPSC lines from a patient-derived PSEN1





int4del iPSC line (Fig. 1). In order to generate an allelic series, a PAM site 6 base pairs upstream of the mutation was selected, recognizing both mutant and wild-type alleles. This enables both homology-directed repair from the ssODN (single-stranded oligodeoxynucleotide) and template-free repair of the pathogenic variant in the same CRISPR/Cas9 transfection (Shen *et al.*, 2018). For increased efficiency of homology-directed DNA repair, the ssODN template was modified to contain phosphorothioate moieties (Renaud *et al.*, 2016).

Following an initial screen of 800 iPSC colonies by RFLP (see Materials and methods section), Sanger sequencing was used to confirm the generation of: (i) an isogenic control cell line, (ii) an unedited line, (iii) a homozygous int4del line and (iv) a *PSEN1* knockout line (Fig. 2A). The knockout line was a compound heterozygous, which contained a 4 and a 25 base pair deletion; each leading to a reading frame shift (Supplementary Fig. 1). The allelic series was screened and found to be free from off-target nucleotide changes at five most likely genomic sites (see Materials and methods section) and pluripotency was confirmed via the expression of OCT4 and SSEA4 (Fig. 2B). Karyotype stability was tested and no

significant aberrations were found (Supplementary Fig. 2). iPSCs were subjected to cortical differentiation, generating the cell type affected by FAD (Shi *et al.*, 2012). All lines generated neurons with a similar efficiency, as evidenced by the expression of the deep-layer cortical marker TBR1 by immunocytochemistry and the population expression level of *TUBB3*, *TBR1* and *CTIP2* by qPCR (Fig. 2C and D). Finally, to confirm the mutation status of the iPSC-derived neurons, cDNA was analysed by PCR to depict aberrant splicing of *PSEN1* in mutation-bearing neurons (Fig. 2E; Tysoe *et al.*, 1998). In addition to the full-length L113\_I114insT encoding transcript (374 bp), heterozygous and homozygous *PSEN1* int4del lines show evidence of one short transcript produced by aberrant splicing (193 bp).

### iPSC-derived *PSEN1* knockout neurons display aberrant APP processing

Using primers 3' to the site of gene editing, qPCR analysis showed reduced *PSEN1* expression in the knockout

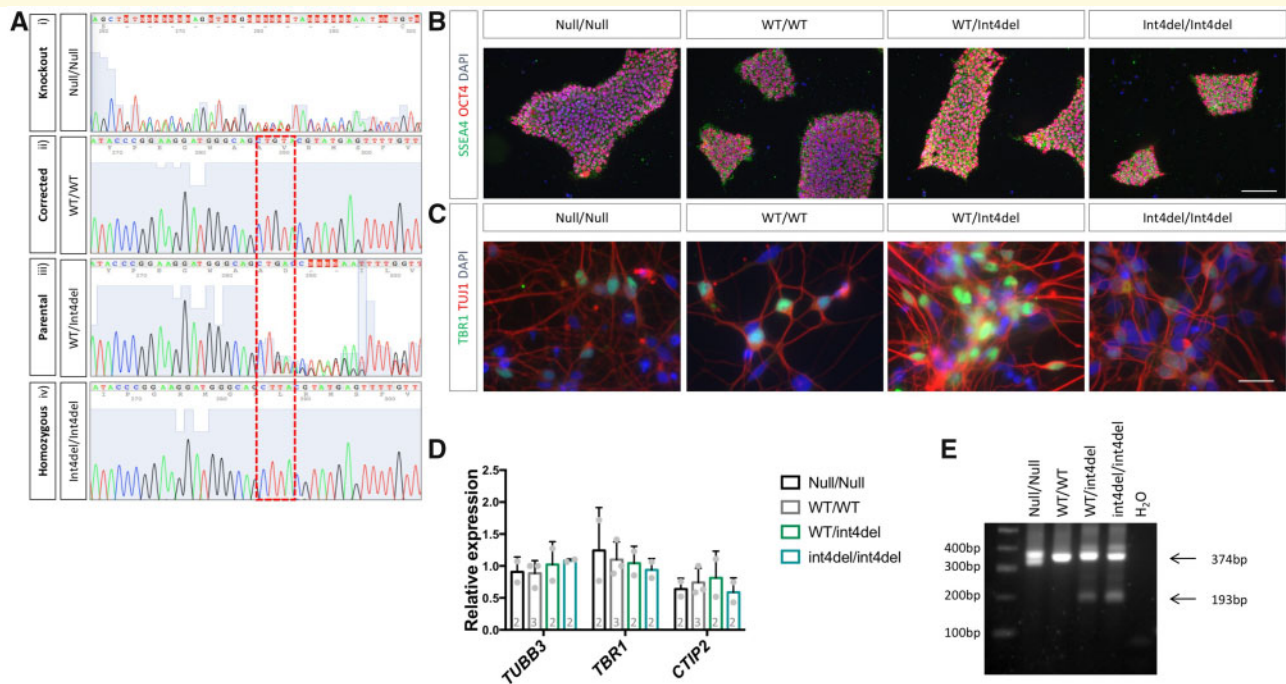


**Figure 2 Characterization of gene-edited iPSC and neurons.** (A) Sanger sequencing was used to confirm the generation of a *PSEN1* knockout (i), a corrected wild-type *PSEN1* line (ii), an unedited heterozygous mutant line (iii) and a homozygous *PSEN1* int4del mutation line (iv). (B) Immunocytochemistry was performed on all iPSC lines following CRISPR/Cas9 editing to confirm pluripotency with the pluripotency markers OCT4 (red) and SSEA4 (green). Scale bar 100  $\mu$ m. (C) Successful differentiation of iPSC into neurons was characterized 50 days post-induction by immunocytochemistry for the neuronal marker TUJ1 (red) and deep-layer cortical neuronal marker TBR1 (green). Scale bar 25  $\mu$ m. (D) Further characterization of cortical differentiation was performed using qPCR analysis 100 days post-neural induction to assess expression of neuronal marker *TUBB3* and cortical layer markers *TBR1* and *CTIP2*. Numbers within histogram represent the number of independent neural inductions. (E) PCR analysis of *PSEN1* splicing in cDNA from day 100 neurons using primers recognizing exons 3 and 5 of *PSEN1* mRNA. The full-length transcript is depicted at 374 bp and one short transcript caused by aberrant splicing is evident at 193 bp in mutation-bearing neurons (we do not see evidence of a second aberrantly spliced band at 111 bp).

cell line (Fig. 3A). Interestingly, *PSEN2* showed similar expression in all cell lines, suggesting that loss of *PSEN1* does not result in compensation by up-regulation of this alternate  $\gamma$ -secretase subunit. Expression of *APP* and *BACE1* was not significantly altered based on mutation status.

At the protein level, the expected absence of *PSEN1* protein was confirmed in the knockout line (using antibodies that recognize the N- or C-terminus of *PSEN1*; Fig. 3B). The *PSEN1* knockout line also showed a reduced maturation of NCSTN, evidenced as a relative lack of the larger band that represents the glycosylated protein (Leem et al., 2002). This phenotype was not seen in lines containing the mutation (Fig. 3C). Similar to qPCR analysis, there was no apparent compensatory up-regulation of *PSEN2* protein in *PSEN1* knockout cells as analysed by western blot (Fig. 3D). Total APP levels were largely equivalent (Fig. 3E and F); however, an accumulation of a fragment predicted to be C99 was present in the *PSEN1* knockout neurons—analogue to  $\gamma$ -secretase-inhibited wild-type cells (Fig. 3E).

## $A\beta$ is produced in knockout cells and disease-associated processing defects are dependent on mutant gene dosage

To investigate the molecular effects of the *PSEN1* int4del mutation, we analysed the  $A\beta$  profiles of the neuronal condition media 100 days post neural induction. *PSEN1* knockout cells produced less  $A\beta$  compared with other lines, reaching significance for  $A\beta_{38}$  (Fig. 4A–C). The levels of  $A\beta$  remained within detection limits, which are in contrast to neurons treated with the  $\gamma$ -secretase inhibitor DAPT, where  $A\beta$  was at or below the detection threshold. Expression of four  $A\beta$  degrading enzymes remains consistent between genotypes (Supplementary Fig. 3), suggesting that the detection of  $A\beta$  is not a result of reduced degradation.

Knockout cells produced a non-significant increase in the  $A\beta_{42:40}$  and  $A\beta_{42:38}$  ratios and a significantly reduced  $A\beta_{38:40}$  ratio when compared with isogenic

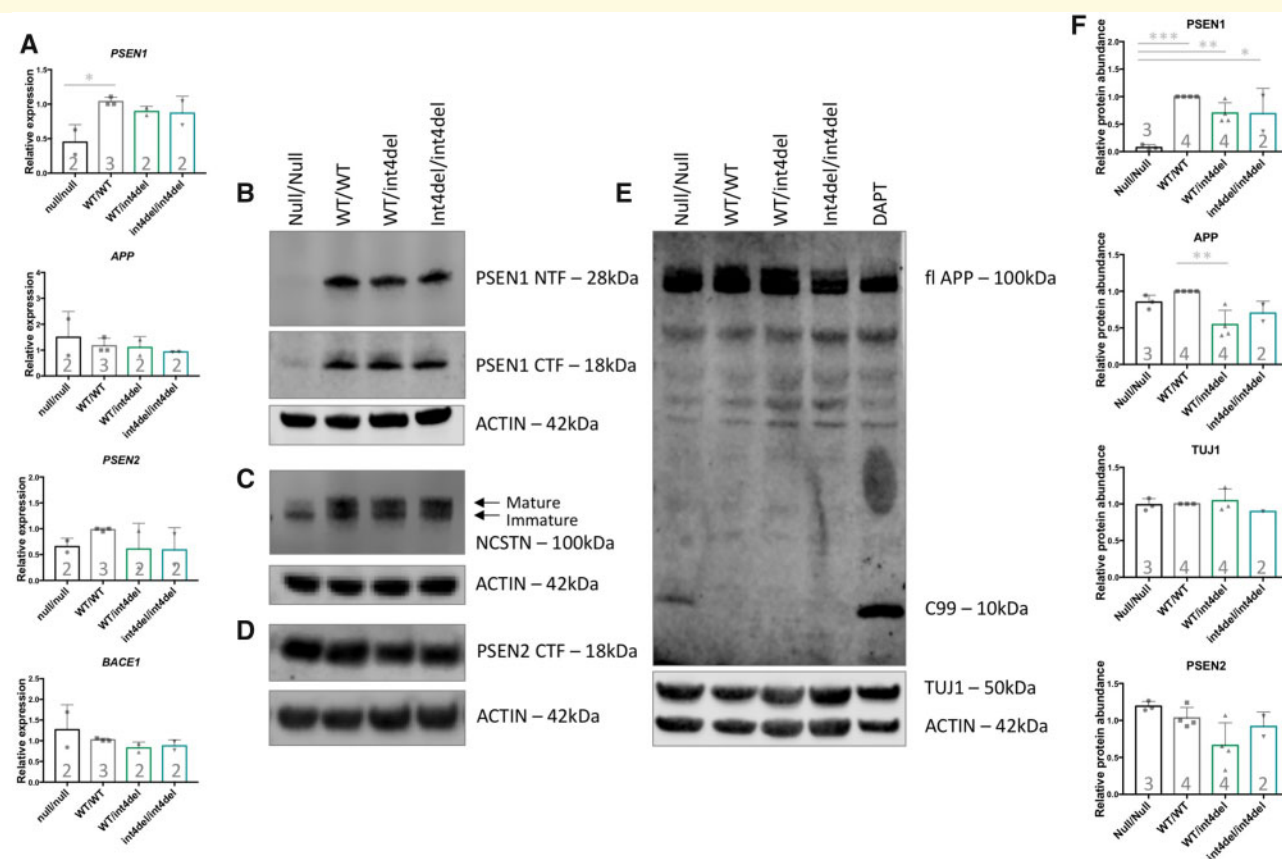


**Figure 3 Analysis of  $\gamma$ -secretase and APP processing in iPSC-derived neurons.** (A) *PSEN1*, *PSEN2*, *APP* and *BACE1* expression in iPSC-derived neurons 100 days post-induction was assessed by qPCR in neurons from *PSEN1* knockout, *PSEN1* wild type, *PSEN1* int4del heterozygous and *PSEN1* int4del homozygous lines. *PSEN1* expression was significantly reduced in the *PSEN1* knockout neurons. No significant differences in *PSEN2*, *APP* and *BACE1* were observed. (B–E) Western blot on whole cell lysates of day 100 neurons was used to analyse protein levels of *PSEN1* N-terminal fragments (28 kDa), *PSEN1* C-terminal fragments (18 kDa), NCSTN (100 kDa), *PSEN2* C-terminal fragments (18 kDa), APP (100 kDa) and neuronal marker TUJ1 (50 kDa). The DAPT sample represents an unrelated control line treated with the  $\gamma$ -secretase inhibitor DAPT at 10  $\mu$ M for 48 h. (F) Quantification of western blot band intensities in B–E. *PSEN1* protein abundance is significantly reduced in *PSEN1* knockout lysates and APP is significantly increased in the corrected wild-type neurons compared with parental *PSEN1* int4del. \* $P > 0.05$ , \*\* $P > 0.01$ , \*\*\* $P > 0.001$  by one-way ANOVA with Tukey's *post hoc* analysis. Numbers within histograms represent the number of independent neural inductions.

control cells (Fig. 4D–F). These changes are analogous to the changes witnessed between the wild type and the heterozygous int4del line.

The heterozygous and homozygous int4del lines showed increased total levels of A $\beta$ 42 and reduced production of A $\beta$ 38 in a gene dosage-dependent manner (Fig. 4A–C). This corresponds to similar stepwise mutant gene dosage-dependent changes to A $\beta$ 42:40, A $\beta$ 42:38 and A $\beta$ 38:40 (Fig. 4D–F). In each instance, the homozygous line was significantly different from the patient-derived heterozygous line.

## Discussion

We successfully generated an isogenic allelic series of the *PSEN1* mutation int4del with which to investigate the molecular mechanisms of FAD mutation-dependent effects on APP processing. We found that *PSEN1* knockout cells

produce low levels of A $\beta$  and that *PSEN1* int4del heterozygous and homozygous cells produce a stepwise increase in longer, disease-associated A $\beta$  peptides.

It is intriguing that *PSEN1* knockout neurons produce small amounts of A $\beta$ . This is in contrast to  $\gamma$ -secretase-inhibited cells where A $\beta$  species are often below the detection limit but in agreement with the detection of around one-fifth of total A $\beta$  levels in mouse *PSEN1* knockout primary neurons (De Strooper *et al.*, 1998). It is noteworthy that A $\beta$  is barely detectable after  $\gamma$ -secretase administration to patients during clinical trials (Gillman *et al.*, 2010). We provide evidence for no compensatory up-regulation of *PSEN2* at either the transcriptional or protein level, which could potentially be due to alternate subcellular compartmentalization (Sannerud *et al.*, 2016). These data suggest that *PSEN2* may produce low levels of A $\beta$  in neurons. Alternatively, the lack of compensation by *PSEN2* in *PSEN1* knockout neurons, taken together with the reduced functional  $\gamma$ -secretase



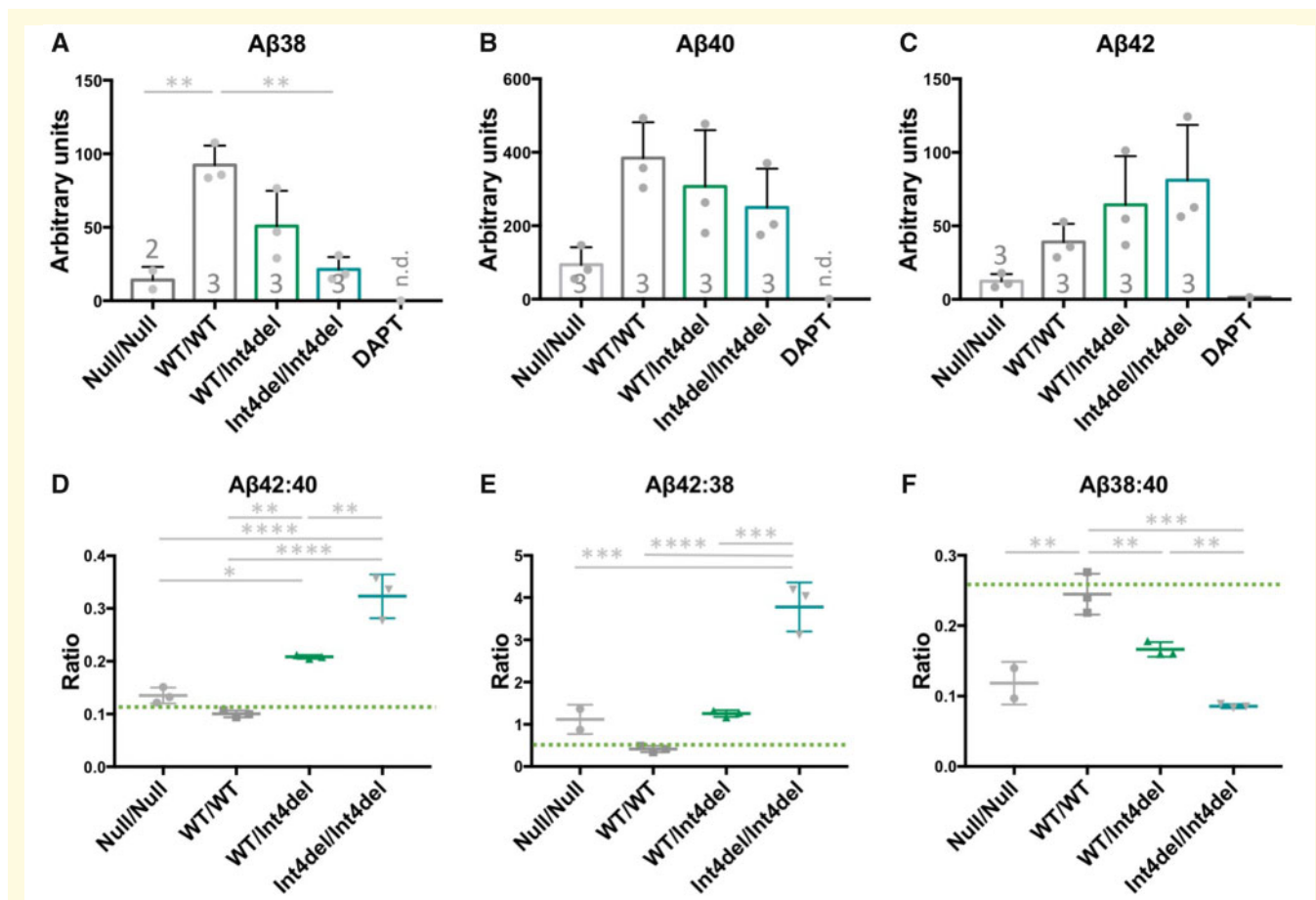


**Figure 4 Aβ analysis in iPSC-neuronal-conditioned media.** (A–C) Quantification of Aβ38, Aβ40 and Aβ42 in 48 h-conditioned media from neurons at day 100, measured by electrochemiluminescence and normalized to total protein content from the cell pellet. The DAPT sample is a representative unrelated control line treated with 10 μM of the γ-secretase inhibitor DAPT for 48 h; n.d., not detected. Numbers within histograms represent the number of independent neural inductions. (D–F) Aβ ratios to depict the disease-associated Aβ42:40 ratio, γ-secretase carboxypeptidase-like activity Aβ42:38 and endopeptidase cleavage position choice Aβ38:40.  $n=3$  for each sample apart from where Aβ38 was below detection limit for one null/null sample. Green bars represent non-Alzheimer's disease neuronal ratios from Arber et al. (2019). \* $P > 0.05$ , \*\* $P > 0.01$ , \*\*\* $P > 0.001$  and \*\*\*\* $P > 0.0001$  by one-way ANOVA with Tukey's *post hoc* analysis.

pool, seen via NCSTN immaturity, promotes the hypothesis that alternative Aβ-generating enzymes are contributing to Aβ production in PSEN1 knockout human neurons. This hypothesis is reinforced as Aβ is detectable in PSEN1 and PSEN2 double knockout mice (Wilson et al., 2002). It should be noted that in non-neuronal cells, knockout of either PSEN1 or PSEN2 does not alter total Aβ generation, whereas double knockout drastically reduces total Aβ (Lessard et al., 2019). Candidates for C-terminal Aβ degrading activity include matrix metalloproteinase 2 or 9 (MMP2/9; Hernandez-Guillamon et al., 2015) and cathepsin B (Mueller-Stieber et al., 2006).

The finding that PSEN1 knockout cells have a relative increase in Aβ42 compared with Aβ38 means that variability in PSEN1 expression levels could contribute to altered Aβ profiles in Alzheimer's disease.

It is important that int4del homozygous cells display an additional, stepwise increase in disease-associated Aβ profiles compared with the patient-derived lines. This equates

to a linear increase in total Aβ42 production. Our data demonstrate a mutant gene dosage-dependent effect in Aβ42 generation reinforcing similar findings with the PSEN1 exon 9 mutation (Woodruff et al., 2013), the PSEN1 M146I mutation (Paquet et al., 2016) and recently 7 fAD mutations investigated by genome editing (Kwart et al., 2019). The PSEN1 knockout neurons and mutation-bearing neurons show different phenotypes with respect to quantitative production of Aβ and, taken together with the dissimilar effects on C99 accumulation and NCSTN maturation, these data argue against a simple loss-of-function mechanism for PSEN1 mutations. In agreement with these findings and in contrast to fAD-causing mutations, PSEN1 loss-of-function mutations have been found to cause acne inversa rather than dementia (Wang et al., 2010).

The fact that PSEN1 int4del homozygosity does not lead to altered NCSTN maturation, suggests that the effect of the mutation acts on γ-secretase as a whole and



not on the activity of PSEN1 itself. This is reinforced by recent crystal structure findings (Yang *et al.*, 2019; Zhou *et al.*, 2019) and mechanistic studies (Szaruga *et al.*, 2017; Petit *et al.*, 2019) whereby fAD mutations appear to destabilize substrate to holo-enzyme complex interaction to release longer A $\beta$  fragments before complete enzymatic processing, rather than altering the PSEN1 subunit activity.

The fact that APP protein is significantly increased in the isogenic control compared with the parental PSEN1 int4del heterozygous line is intriguing. In our previous work, total APP is not significantly altered in the patient-derived line versus unrelated controls (Arber *et al.*, 2019). We believe the slight increase in APP total levels in the corrected line may directly relate to the correction of the mutation.

In conclusion, data from this isogenic human neuronal allelic series reinforce the findings that fAD-associated mutations in PSEN1 lead to accumulation of A $\beta$  by reducing the processivity of APP by  $\gamma$ -secretase. Mutations reduce carboxypeptidase-like activity, releasing longer amyloidogenic A $\beta$  peptides in a gene dose-dependent manner. PSEN1 knockout cells generate A $\beta$  and also show distinct substrate processing alterations from int4del homozygous cells, potentially separating  $\gamma$ -secretase-dependent and independent functions of PSEN1 and arguing against a simple loss-of-function mechanism. These findings support a destabilization of  $\gamma$ -secretase-substrate interaction by the mutation; information that is valuable for the design of novel therapeutics.

## Supplementary material

Supplementary material is available at *Brain Communications* online.

## Acknowledgements

We would like to thank the research participants for their time and involvement in the research and Mr Jamie Mitchell for rescuing a crucial vial of cells.

## Funding

This research was supported by the National Institute for Health Research University College London Hospitals Biomedical Research Centre and the Leonard Wolfson Experimental Neurology Centre. The work was also partly supported by the UK Dementia Research Institute at UCL. C.A. is supported by a fellowship from the Alzheimer's Society (AS-JF-18-008) and S.W. is supported by an Alzheimer's Research UK Senior Research Fellowship (ARUK-SRF2016B-2). N.S.R. is supported by a University of London Chadburn Academic Clinical Lectureship in Medicine. N.C.F. acknowledges the support of the UK

Dementia Research Institute at UCL. This work was also supported by the UK Medical Research Council funding to the MRC Dementia Platform UK (MR/M02492X/1) and Medical Research Council core funding to the High-Content Biology Platform at the MRC-UCL LMCB university unit (MC\_U12266B).

## Competing interests

The authors report no competing interests.

## References

- Arber C, Toombs J, Lovejoy C, Ryan NS, Paterson RW, Willumsen N, et al. Familial Alzheimer's disease patient-derived neurons reveal distinct mutation-specific effects on amyloid beta. *Mol Psychiatry* 2019; 1–13. doi:10.1038/s41380-019-0410-8.
- Chávez-Gutiérrez L, Bammens L, Benilova I, Vandersteen A, Benurwar M, Borgers M, et al. The mechanism of  $\gamma$ -secretase dysfunction in familial Alzheimer disease. *EMBO J* 2012; 31: 2261–74.
- De Jonghe C, Cruts M, Rogeava EA, Tysoe C, Singleton A, Vanderstichele H, et al. Aberrant splicing in the presenilin-1 intron 4 mutation causes presenile Alzheimer's disease by increased Abeta42 secretion. *Hum Mol Genet* 1999; 8: 1529–40.
- De Strooper B, Saftig P, Craessaerts K, Vanderstichele H, Guhde G, Annaert W, et al. Deficiency of presenilin-1 inhibits the normal cleavage of amyloid precursor protein. *Nature* 1998; 391: 387.
- De Strooper B. Aph-1, Pen-2, and nicastrin with presenilin generate an active  $\gamma$ -secretase complex. *Neuron* 2003; 38: 9.
- Gillman KW, Starrett JE, Parker MF, Xie K, Bronson JJ, Marcin LR, et al. Discovery and evaluation of BMS-708163, a potent, selective and orally bioavailable  $\gamma$ -secretase inhibitor. *ACS Med Chem Lett* 2010; 1: 120–4.
- Haapasalo A, Kovacs DM. The many substrates of presenilin/ $\gamma$ -secretase. *J Alzheimers Dis* 2011; 25: 3–28.
- Hardy J, Allsop D. Amyloid deposition as the central event in the aetiology of Alzheimer's disease. *Trends Pharmacol Sci* 1991; 12: 383.
- Hernandez-Guillamon M, Mawhirt S, Blais S, Montaner J, Neubert TA, Rostagno A, et al. Sequential amyloid- $\beta$  degradation by the matrix metalloproteases MMP-2 and MMP-9. *J Biol Chem* 2015; 290: 15078–91.
- Hodgkins A, Farne A, Perera S, Grego T, Parry-Smith DJ, Skarnes WC, et al. WGE: A CRISPR database for genome engineering. *Bioinformatics* 2015; 31: 3078.
- Kwart D, Gregg A, Scheckel C, Murphy E, Paquet D, Duffield M, et al. A large panel of isogenic APP and PSEN1 mutant human iPSC neurons reveals shared endosomal abnormalities mediated by APP  $\beta$ -CTFs, not A $\beta$ . *Neuron* 2019; 1–15. [Epub ahead of print].
- Leem JY, Vijayan S, Han P, Cai D, Machura M, Lopes KO, et al. Presenilin 1 is required for maturation and cell surface accumulation of nicastrin. *J Biol Chem* 2002; 277: 19236–40.
- Lessard CB, Rodriguez E, Ladd TB, Minter LM, Osborne BA, Miele L, et al. Individual and combined presenilin 1 and 2 knockouts reveal that both have highly overlapping functions in HEK293T cells. *J Biol Chem* 2019; 294: 11276.
- Matsumura N, Takami M, Okochi M, Wada-Kakuda S, Fujiwara H, Tagami S, et al.  $\gamma$ -Secretase associated with lipid rafts: multiple interactive pathways in the stepwise processing of  $\beta$ -carboxyl-terminal fragment. *J Biol Chem* 2014; 289: 5109–21.
- Moore S, Evans LDB, Andersson T, Portelius E, Smith J, Dias TB, et al. APP metabolism regulates tau proteostasis in human cerebral cortex neurons. *Cell Rep* 2015; 11: 689–96.
- Mueller-Steiner S, Zhou Y, Arai H, Roberson ED, Sun B, Chen J, et al. Anti-amyloidogenic and neuroprotective functions of

- cathepsin B: implications for Alzheimer's disease'. *Neuron* 2006; 51: 703–14.
- Paquet D, Kwart D, Chen A, Sproul A, Jacob S, Teo S, et al. Efficient introduction of specific homozygous and heterozygous mutations using CRISPR/Cas9. *Nature* 2016; 533: 125–9.
- Petit D, Hitznerberger M, Lismont S, Zoltowska KM, Ryan NS, Mercken M, et al. Extracellular interface between APP and nicastrin regulates A $\beta$  length and response to  $\gamma$ -secretase modulators'. *EMBO J* 2019; 38: e101494.
- Renaud J-B, Boix C, Charpentier M, De Cian A, Cochenne J, Duvernois-Berthet E, et al. Improved genome editing efficiency and flexibility using modified oligonucleotides with TALEN and CRISPR-Cas9 nucleases. *Cell Rep* 2016; 14: 2263.
- Ryan NS, Nicholas JM, Weston PSJ, Liang Y, Lashley T, Guerreiro R, et al. Clinical phenotype and genetic associations in autosomal dominant familial Alzheimer's disease: a case series'. *Lancet Neurol* 2016; 15: 1326–35.
- Sannerud R, Esselens C, Ejsmont P, Mattera R, Rochin L, Tharkeshwar AK, et al. Restricted location of PSEN2/ $\gamma$ -secretase determines substrate specificity and generates an intracellular A $\beta$  pool. *Cell* 2016; 166: 193.
- Shen MW, Arbab M, Hsu JY, Worstell D, Culbertson SJ, Krabbe O, et al. Predictable and precise template-free CRISPR editing of pathogenic variants. *Nature* 2018; 563: 646.
- Shi Y, Kirwan P, Smith J, Robinson HPC, Livesey FJ. Human cerebral cortex development from pluripotent stem cells to functional excitatory synapses. *Nat Neurosci* 2012; 15: 477–86.
- Szaruga M, Munteanu B, Lismont S, Veugelen S, Horr   K, Mercken M, et al. Alzheimer's-causing mutations shift A $\beta$  length by destabilizing  $\gamma$ -secretase-A $\beta$ n interactions. *Cell* 2017; 170: 443–56.e14.
- Szaruga M, Veugelen S, Benurwar M, Lismont S, Sepulveda-Falla D, Lleo A, et al. Qualitative changes in human  $\gamma$ -secretase underlie familial Alzheimer's disease. *J Exp Med* 2015; 212: 2003–13.
- Takami M, Nagashima Y, Sano Y, Ishihara S, Morishima-Kawashima M, Funamoto S, et al. Gamma-secretase: successive tripeptide and tetrapeptide release from the transmembrane domain of beta-carboxyl terminal fragment. *J Neurosci* 2009; 29: 13042–52.
- Tysoe C, Whittaker J, Xuereb J, Cairns NJ, Cruts M, Van Broeckhoven C, et al. A presenilin-1 truncating mutation is present in two cases with autopsy-confirmed early-onset Alzheimer disease'. *Am J Hum Genet* 1998; 62: 70–6.
- Veugelen S, Saito T, Saido TC, Ch  vez-Guti  rrez L, De Strooper B. Familial Alzheimer's disease mutations in presenilin generate amyloidogenic A $\beta$  peptide seeds. *Neuron* 2016; 90: 410–6.
- Wang B, Yang W, Wen W, Sun J, Su B, Liu B, et al.  $\Gamma$ -Secretase gene mutations in familial acne inversa. *Science* 2010; 330: 1065.
- Wilson CA, Doms RW, Zheng H, Lee VM-Y. Presenilins are not required for A $\beta$ 42 production in the early secretory pathway. *Nat Neurosci* 2002; 5: 849–55.
- Woodruff G, Young JE, Martinez FJ, Buen F, Gore A, Kinaga J, et al. The presenilin-1  $\Delta$ E9 mutation results in reduced  $\gamma$ -secretase activity, but not total loss of PS1 function, in isogenic human stem cells. *Cell Rep* 2013; 5: 974–85.
- Xia D, Kelleher RJ, Shen J. Loss of A $\beta$ 43 production caused by presenilin-1 mutations in the knockin mouse brain. *Neuron* 2016; 90: 417–22.
- Yang G, Zhou R, Zhou Q, Guo X, Yan C, Ke M, et al. Structural basis of Notch recognition by human  $\gamma$ -secretase. *Nature* 2019; 565: 192–7.
- Zhou R, Yang G, Guo X, Zhou Q, Lei J, Shi Y. Recognition of the amyloid precursor protein by human  $\gamma$ -secretase. *Science* 2019; 363: eaaw0930. [Epub ahead of print]. doi:10.1126/science.aaw0930.